SAND81-1231
Unlimited Release
Printed September 1981

A SOLUTION MINING CODE FOR STUDYING AXISYMMETRIC SALT CAVERN FORMATION

A. J. Russo
Sandia National Laboratories
Albuquerque, New Mexico 87185

ABSTRACT

The solution mining of oil storage caverns in salt domes for the Strategic Petroleum Reserve has prompted the development of a code to predict cavern shape and volume as a function of prescribed flow parameters. Of particular interest is the ability to predict shape changes while leaching is proceeding at the same time the cavern is being filled with oil (leach-fill) and when oil is being withdrawn by fresh water displacement. The theory and overall numerical procedures used in the code development are described. Implicit, finite difference methods are used to solve an axisymmetric mass conservation problem. Calculated results are given which exercise each of the code options and where possible these results are compared with other calculations or available data from solution mining in progress at Bryan Mound, Texas.

This report is not a users manual for the code.

TABLE OF CONTENTS

LIST OF FIGURES

NOMENCLATURE

A	Cavern horizontal cross sectional area
b	Local effective plume radius
C	Local fluid specific gravity
C_o	Brine specific gravity outside the plume region
$\hat{C}$	Brine specific gravity at maturation
C^*	Brine specific gravity at the next time step
C_{salt}	Specific gravity of rock salt
C_p	Brine Specific gravity at the production level
d	Differential operator
D	Total diffusion coefficient of salt in water
D_e	Eddy diffusion coefficient
D_{mol}	Molecular diffusion coefficient
D_o	An empirical parameter used to calculate D_e
f	Ratio of the change in specific gravity to the change in weight percent
FSG	Specific gravity as a function of weight percent of salt
FWP	Weight percent as a function of specific gravity
g	Acceleration of gravity
i	Positional subscript in the z direction in difference expressions
I	Mesh interval summation index
ℓ	Mixing length
m_{co}	Initial mass of brine in a cavern
M_c	Total brine mass calculated from a sum of height interval masses at a given time
M_o	Volume flow rate caused by pumping
M_T	Total brine mass calculated from a cavern flow history

N	Number of mesh intervals used to model a cavern
Q_{fill}	Oil volume flow rate
Q_i	Injection volume flow rate
Q_o	Outlet volume flow rate of brine for no oil flow
r	Cavern radius
R	General enclosure radius
s_d	Salt dissolution coefficient
t	Time
T	Total time period
U	Vertical plume velocity
U_{max}	Maximum plume velocity
V	Volume increment
VSR	Volume of salt removed by dissolution in one time increment
w	Weight percent of salt in brine
z	Vertical coordinate
α	Fluid entrainment coefficient
Δ	Prefix denoting incremental quantity
ξ	Coordinate normal to a surface
θ	Wall angle measured from the vertical
λ	Instability wavelength
ν	Fluid dynamic viscosity
π	3.141592653

I. INTRODUCTION

The United States Strategic Petroleum Reserve (SPR) consists of an underground oil storage system which uses caverns which have been leached in salt domes near the Gulf of Mexico and a former salt mine on Weeks Island, Louisiana. Some of the cavern space, formed during commercial brining operations, was available for storage shortly after the program began: however, since this space was less than 250 million barrels and storage of up to 1 billion barrels of oil has been contemplated, the DOE has undertaken an extensive new cavern leaching program.

Sandia National Laboratories has, since the end of 1978, been serving as a technical consultant to the DOE on various aspects of the SPR program including the leaching project. One of the tools used to predict cavern development and formulate leaching schedules has been a computer code, SALT77, developed for the Solution Mining Research Institute by Ahmed Saberian and A. L. Podio.[1] This code has been very useful for planning some portions of the leaching program however it has the following disadvantages: it does not permit modeling of leaching during oil withdrawal without an approximate and tedious sequencing of runs: it cannot be used in a no-flow case to estimate cavern growth during the period that the cavern fluid goes to saturation: and the explicit numerical formulation used necessitates a time step limitation which causes impractically long running times for some configurations.

Aside from the above functional disadvantages, it is sometimes desirable to modify the solution mining code to meet new or

changing needs of the mining operation. The empirical models used in the SMRI code and its structure make it difficult to modify without extensive familiarization. To overcome these problems a new solution mining code is being developed at Sandia National Laboratories. This report describes the models used in the new code and gives some results of applications to SPR cases.

II. THEORY

Basic Equations

Figure 1 shows the configuration to be considered in cavern leaching. Fresh water (or water of low salinity) is assumed to enter the cavern at the injection level. In Figure 1, this level is below the brine production level (direct leaching), however, the injection and production levels may be interchanged by switching the water and brine connections at the surface (reverse leaching). In either case the fresh water injected will be less dense than the cavern brine and will, because of buoyant forces form an upward moving plume. Since the mixing within the plume is usually rapid an analysis of plume dynamics based on the assumption of a uniform specific gravity and velocity within the plume (top hat model) is appropriate. Reference 2 presents the results of such an analysis as a set of equations which describe the dynamics of an unconstrained steady plume.

$$\frac{d\,(b^2\,u)}{de} = 2\alpha b u$$

$$\frac{d\,(b^2\,u^2)}{dz} = 2\,b^2 g\,(C_0 - C) \qquad (1)$$

$$\frac{d\,(b^2\,ug\,(C_o - C))}{dz} = 2\,b^2\,ug\,\frac{d\,C_o}{de}$$

where b is the effective plume radius

C and C_o are fluid specific gravities in and out of the plume

u is the plume velocity in the vertical (z) direction

g is the acceleration of gravity

and a is an entrainment coefficient.

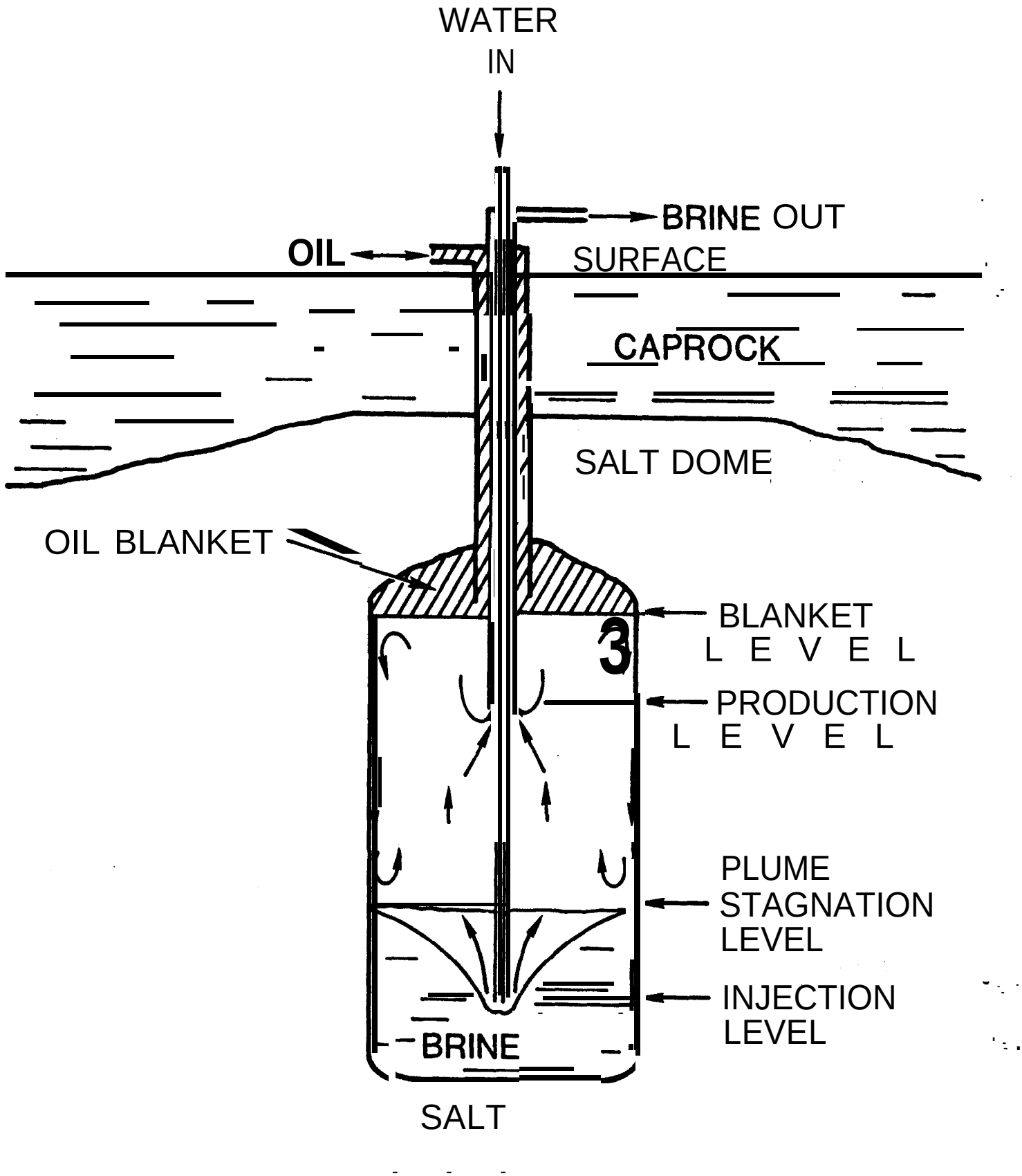

Figure 1. Cavern Geometry and Flow Regfons for Direct Leaching

When the plume is rising through a stably stratified fluid ($\partial c_o/\partial z < 0$) it will rise to a certain level and stop, and its radius will grow indefinitely. This level is denoted by the plume stagnation level in Figure 1. If the plume is rising in an unstably stratified fluid it will continue to rise and grow until it interacts with the cavern walls which then constrain the plume and change its rise rate. The level at which this interaction occurs will also be denoted as the plume stagnation level, because in either case the entire plume flow is deposited in the fluid cell containing this level.

If the plume stagnation level is above the production level the cavern fluid will flow downward at an average velocity determined by the injection rate and the cavern radius. Since the injected fluid is less dense, the region below the stagnation and production levels (exclusive of the plume) will be stably stratified. If the stagnation level is below the production level (as shown in Figure 1) the net cavern flow will be upward and the fluid above the stagnation level will'be quasi-stable, and below it, stable. Quasi-stable means that even though the density gradient is unstable, with the heavier fluid on top, the wall constraints and the large length to diameter ratios generally prevalent in caverns being leached, prevent large scale rapid mixing or rollover from occurring. A large number of small scale Raleigh instabilities are likely to occur that give rise to a mixing which it has been assumed can be described by an enhanced diffusion coefficient.

All the fluid in the cavern, except for a small region of plume rise between the injection and stagnation levels, and a thin boundary layer region next to the surface, will be stable or quasi-stable for all cases. Rahm and Walin[3,4,5] have developed an approximate theory for treating combined natural and forced convection in stably stratified enclosures where the natural convection is induced by wall sources weak enough so that the thermal or concentration boundary layer variations are smaller than the total variation due to stratification. The result of this analysis is that the variation of specific gravity, C, with height in the bulk of the fluid is given by Equation (2) for axisymmetric caverns.

$$\frac{\partial C}{\partial t} + \left(\frac{M_o}{A} - \frac{2D}{r}\frac{dr}{dz}\right)\frac{\partial C}{\partial z} + \frac{2DS_d\,(C - \hat{C})}{r\cos\theta} = D\,\frac{\partial^2 C}{\partial z^2} \qquad (2)$$

where M_o is the total externally induced volume flow rate

A is the cavern cross sectional area

D is the diffusion coefficient of salt in water

r is the cavern radius

S_d is a source coefficient defining the wall boundary condition by $\left.\frac{\partial C}{\partial \xi}\right|_{\xi=0} = S_d\,(C - \hat{C})$

$\hat{C}$ is the specific gravity of the fluid at the wall ($\xi = 0$). Taken to be the saturation value of 1.202

t is time

and θ is the wall angle with respect to vertical.

Equation (2) is a mass conservation equation which sets the rate of salinity increase (first term) equal to the sum of the net

convective flux (second term), the rate of salt dissolution at the walls (third term) and the diffusive flux (last term).

Relaxation of the stable stratification restriction to a quasi-stable one will primarily affect the area change portion of the convective term which, in a leaching situation, is small compared to the external convection. It will therefore be assumed that Equation (2) is applicable throughout the cavern, with a diffusion coefficient that is a function of position.

In order to evaluate the boundary source coefficient, S_d, empirical salt dissolution models were used. Data on salt dissolution rates was taken at the University of Texas in the 1960s,[6,7] and some of the results are summarieed in Reference 1.

The recession rate of a large vertical wall of salt dissolving under the influence of natural convection can be correlated as a function of the bulk fluid specific gravity, C, alone at temperatures near 70°F.

$$\frac{dr}{dt} = 45.654996\ C^4 - 232.29310\ C^3 + 469.52470\ C^2 - 470.37554\ C + 232.73686 - 45.203241\ /C \text{ ft/hr} \quad (3)$$

The recession rate varies with wall angle, θ, measured from the vertical so that $\theta = 90$ is an upward facing surface and $\theta = -90$ is a downward facing surface, according to:

$$\left.\frac{dr}{dt}\right|_{\theta>0} = \left.\frac{dr}{dt}\right|_{\theta=0} [\cos\theta]^{1/2}$$

$$\left.\frac{dr}{dt}\right|_{\theta<0} = \left.\frac{dr}{dt}\right|_{\theta=0} \left\{1 + 0.22 \left[1 - \sqrt[3]{\frac{\theta + 45'}{45°}}\right]\right\} \quad (4)$$

The volume of salt removed, VSR, from a height increment, dz, in a time, At, is

$$VSR = 2\pi r dz \frac{dr}{at} At \tag{5}$$

To interpret the change of specific gravity in terms of the volume of salt removed, two functions are defined: EWP, which gives the weight percentage of salt as a function of specific gravity, and its inverse FSG. The mass of salt dissolved in a volume, V, of cavern fluid of specific gravity, C, is CV FWP(C).* The mass of salt removed is VSR C_{salt}, where C_{salt} is the specific gravity of rock salt (=2.16). The new weight percent, w, of salt after dissolution of additional salt is

$$w = \frac{(CV\ FWP(C) + VSR\ C_{salt})}{(CV + VSR\ C_{salt})} \tag{6}$$

and the specific? gravity rate of change is,

$$\frac{dC}{dt} = \frac{FSG(w) - C}{At} \quad . \tag{7}$$

Substituting (7) into (2) for the case of constant zero salinity gradient permits evaluation of s_d in terms of the salt removal rate.

$$s_d = \frac{[FSG(w) - Cl\ r\ \cos\theta}{2\ D\ At\ (\bar{C} - C)} \tag{8}$$

The cavern fluid through which the plume flows loses salt by entrainment into the plume. This loss mechanism is not accounted

* All masses are normalized by the density of water.

for in Equation (2), therefore an additional sink term should be included in Equation (2). Although such a term has been included in the coding, the best way to evaluate it is not clear. At present, the sink term is set to zero and the plume injection flow at the stagnation level is set to the inlet injection rate and specific gravity. That is, after determining the appropriate stagnation level from plume theory (Equation (1)), the code behaves as though the fresh water were injected and mixed directly at the stagnation level. This approximation should cause more dissolution at the stagnation level and less below it, however comparison with calculations employing a different sink model showed little difference for the reverse leaching case. For the direct leaching case where the bulk flow is all upwards, the neglect of the sink term would result in a large stable gradient between the injection and stagnation level. This gradient would restrict the distance between the injection and stagnation levels to approximately $0.155Q_i^{0.4}$ feet where Q_i ft^3/hr is the injection flow rate.[2] For most SPR problems this distance is less than one mesh space, so to save computational time and avoid a numerical plume oscillation problem, the stagnation level has been assumed to coincide with the injection level for all direct leaching cases. Since there will always be significant mixing between the injection and stagnation levels due to convective return of entrained fluid it is expected that this will be a good approximation for most cases.

Diffusion Coefficient

The diffusion of salt through water by thermo-molecular processes is very slow, having a molecular diffusion coefficient of

5.4×10^{-5} ft^2/hr (1.4×10^{-5} cm^2/sec). When an unstable salinity gradient exists any disturbance will grow into a plume which, in an unbounded region with a constant gradient can be described by[8]

$$u = \sqrt{g \frac{dC_o}{dz}} \frac{z}{4} \qquad \text{a.}$$

$$C - C_0 = \frac{1}{4} \frac{dC_o}{dz} z \qquad \text{b.} \qquad (9)$$

$$b = \frac{2}{3} \alpha z \qquad \text{c.}$$

where the symbols are defined in Equation (1). It is seen from (9) that the velocity, density difference and plume radius all increase with vertical distance, z. If the plume is confined, Equations (9) can only describe the plume growth until the plume radius, b, becomes a significant fraction of the confining length. At this point the backflow required by mass conservation limits the plume growth. For example, in a vertical cylindrical tube of radius R the backflow velocity will equal the plume velocity when the plume radius becomes $R/\sqrt{2}$. A large departure of the backflow velocity from zero or low ambient velocity invalidates Equations (9) and there will be some limiting plume radius and velocity which is proportional to the confining radius. After the plume reaches this limiting radius its velocity and buoyancy will decay due to turbulent entrainment and diffusion. Letting the plume radius, b, be proportional to R and combining (9) a and c

$$u_{max} \sim \left(\frac{dC_o}{dz}\right)^{1/2} R \qquad (10)$$

By analogy with molecular diffusion, an eddy diffusion coefficient may be defined as the product of velocity and a mixing length, ℓ, so that

$$D_e \sim \left(\frac{dC_o}{dz}\right)^{1/2} R\ell \qquad (11)$$

If it is assumed that the mixing length is also proportional to R Equation (11) becomes

$$D_e = D_o \left(\frac{dC_o}{dz}\right)^{1/2} R^2 \qquad (12)$$

where D_o is a proportionality constant. Experiments on downward salt diffusion in 2 and 4 inch vertical tubes,' indicate that indeed the diffusion coefficient does scale with the tube radius squared and $D_o \approx 31.7$ $ft^{1/2}/sec$.

When the confining radius becomes very large the instability growth is limited not by the confining walls but by adjacent convection cells. The wavelength of the fastest growing instability determines the size of these cells. A simple estimate of the wavelength of the fastest-growing instability of a thick layer of high density fluid overlaying a lower density fluid is,[10]

$$\lambda = 4\pi\left(\frac{\nu^2}{\frac{\Delta C}{2C} g}\right)^{1/3} \qquad (13)$$

where λ is the wavelength, ν the kinematic viscosity of the two layers and ΔC is the difference in specific gravity of the two layers. To estimate the wavelength for the constant gradient case, AC of Equation (13) is replaced by $\frac{dC}{dz}\ell$, where ℓ is the vertical mixing length.

$$\lambda = 4\pi\left(\frac{2\nu^2 C}{\frac{dC}{dz} g\ell}\right)^{1/3} \qquad (14)$$

Two point instabilities separated by λ should coalesce, according to Equation (9c) when

$$\lambda = \frac{2}{3}\alpha\ \ell \quad .$$

so that from (14)

$$\ell = \left(\frac{6\pi}{\alpha}\right)^{3/4} \left(\frac{2\nu^2 C}{\frac{dC}{dz} g}\right)^{1/4} \qquad (15)$$

If it is assumed that the eddy diffusion coefficient is proportional-to the product of velocity and mixing length, as was done in developing Equation (12) and the mixing length is taken as the minimum of cavern radius r, and ℓ (as given in (15))

$$D_e = D_o \ \ dC/dz \ \text{Min}\ (r^2, \ell^2). \qquad (16)$$

Equation (16) is the final form of the eddy diffusion coefficient to be used in Equation (2) where $D = D_{mol} + D_e$. The value of D_o used was 31.7 $ft^{1/2}/sec$ taken from the data of reference 9, and the value of a in Equation (15) which best fit a limited amount of data taken from Bryan Mound well 104 was 0.064. This value of a is not far from other experimentally determined values for. buoyant plumes and jets which vary between 0.08 and 0.13.[2,11]

Numerical Method

The cavern space to be solution mined is divided into N vertical increments with a mesh point located at each of the N + 1 boundary planes. All values within an increment are assumed to be represented by the value at its lower boundary. The initial radii and concentrations for each increment, the oil-brine interface level, injection and production levels, and the injection flow rate are defined for each case.

At every third time step the Equations (1) are solved, using the Sandia system library integration routine ODERT, for the plume concentration, flow rate, and stagnation level. At each time step the concentration in the mesh increment containing the stagnation level is updated by a mass balance between the injected fluid, the remaining brine in the increment volume, and the salt which diffused and dissolved during one time step. This concentration serves as one of the boundary values for the solution of Equation (2) above and below the stagnation level.

All the terms except the convective one in Equation (2) are implicitly center differenced in conservation form. Upwind differencing is used on the convective term. The difference equations are solved with a tridiagonal algorithm. The diffusion coefficient is a function of concentration gradient and is calculated by

$$D = D_{mol} + D_o \left(\frac{dC}{dz}\right)_+^{1/2} \text{Min}(r, II) \qquad (17)$$

where D_{mol} is the molecular diffusion coefficient, (dC/dz)+ is the specific gravity gradient when positive, and is zero when

the specific gravity gradient is negative. The coefficient D_o is an empirically determined eddy diffusion parameter, and the mixing length ℓ is determined from Equation (16) with $a = 0.064$.

After the solution of Equation (2), the new concentrations are used to calculate the wall recession rate and volume of salt removed from Equations 3, 4 and 5. The cavern radii are updated and the coefficients of Equation (2) reevaluated in preparation for the next time step.

Since the plume Equations (1) and the concentration Equation (2) are tightly coupled and solved sequentially, some numerical oscillation or bouncing of the plume stagnation level can occur. In order to stabilize the plume and limit the errors due to this oscillation, the stagnation level has been restricted to lie within one mesh interval of the level previously calculated (it can change by only one space at a time). Since the time required for the plume to find a stable level is small compared to the leaching time, this approximation should introduce little error.

Boundary Conditions

Although only two boundary conditions are necessary to solve Equation (2) it was found that convective source terms could be included most conveniently by dividing the computational domain into regions above and below the plume stagnation level. The fluid specific gravity at the stagnation level is used as a boundary condition for Equation (2) in these two regions, and is found by doing a mass balance in the stagnation cell between injected fluid, remaining fluid, disolved and diffused salt. Specifically the stagnation level specific gravity for the next time

interval, c_j^*, is computed by Equation (18),

$$c_j^* = c_j + D\frac{\Delta t}{\Delta z^2}(c_{j+1} - c_j^*) + \frac{Q_i\,\Delta t}{V}[c_i - c_{j\pm1}] + \frac{VSR}{VC}c_{salt}\,f \qquad (18)$$

where Q_i is the injection fluid volume flow rate

c_i is the injection fluid volume specific gravity

V is the volume increment at the stagnation level

f is the ratio of $\Delta C/\Delta w$, taken to be $\sim$ 0.777

and other quantities are as previously defined. Only the gradient at the upper boundary is used in the diffusion term (second term on the right) because the region below the stagnation level is assumed to be stably stratified and have negligible diffusion. The plus and minus sign in the convective term (third term) subscript is for direct or reverse leaching respectively. The last term accounts for the change in specific gravity due to the dissolution of salt. The boundary condition at the upper boundary (oil blanket) is a zero derivative condition on the specific gravity corresponding to no flux across this boundary. At the lower boundary a mass balance is done similar to that at the stagnation level. If the *atagnation* level coincides with the upper or lower boundary its calculated boundary value supercedes the others.

The solution to any differential equation is determined by its boundary conditions. The boundary condition at the stagnation level is computed at each time step from the values at the previous time step and errors tend to accumulate. The cavern volume and

shape are very sensitive to the boundary values used, so it is important to limit the errors on these values. This is accomplished by performing a global mass balance at each time step and computing a correction factor for the concentrations and boundary conditions to be used in the next time step. This forces the time integration to follow a self-consistent and self-correcting path.

The total mass of brine in the cavern, MT, is computed by the time integral

$$M_T = m_{co} + \int_o^T \left(\sum_1^N \frac{VSR}{at} C_{salt} + Q_i C_i - (Q_o + Q_{fill}) Cp \right) dt \quad (19)$$

where Q_o is the outlet volume flow rate for no oil flow

Q_{fill} is the oil volume flow rate

C_p is the brine S.G. at the production level

T is the time period

m_{co} is the initial mass of brine in the cavern

and N is the number of mesh intervals used.

The total mass of brine in the cavern, M_c, is computed by

$$M_c = \sum_{I-1}^{N} \pi r(I)^2 \Delta z \, C(I) \quad (20)$$

the correction factor for the stagnation level boundary condition is then found by

$$\text{Corr. Fac} = \frac{M_T}{M_C} \quad (21)$$

This factor is always close to 1 and is printed out with each result. A value of 1 for the correction factor only means, of

course, that the calculation is self-consistent, and not that it is modeling any physical situation correctly.

RESULTS

In order to test the performance of the new solution mining code comparisons were made between cavern shapes calculated with the new code and the SMRI code for several cases. Where possible, comparisons between measured data have also been made.

Comparison With SALT77

The SMRI code has been verified for the cases of bottom injection and brine removal at the top (direct leaching) and top injection and bottom brine removal (reverse leaching).' Since a degree of confidence has been established for the SMRI code for the simple direct and reverse leaching cases, the first comparison to be made will be for leaching a 0.625 foot radius borehole in the direct mode for 40 days at a flow rate of 10603.5 $ft^3/hour$ (1322 gallons/minute) of water with an S.G. of 1.0108, and then in the reverse mode at the same flow rate for 100 days. Figure 2 shows a comparison of the cavern shapes calculated with the SMRI code and the new code. The cavern shapes are almost identical differing only near the injection region by about 10%. The overall cavern volumes differed by 5.5% at the end of the mining process. The produced brine saturation percent differed by less than 0.3%.

Bryan Mound Cavern 106

Some data is available from the direct leaching of Bryan Mound Cavern 106. Two wells, A and B were simultaneously leached for one day at a flow rate of 15078 ft^3/hr, then for.84 days at an average flow rate of 6596 ft^3/hr. The injection water was assumed to have a specific gravity of 1.0108. A 7-inch injection

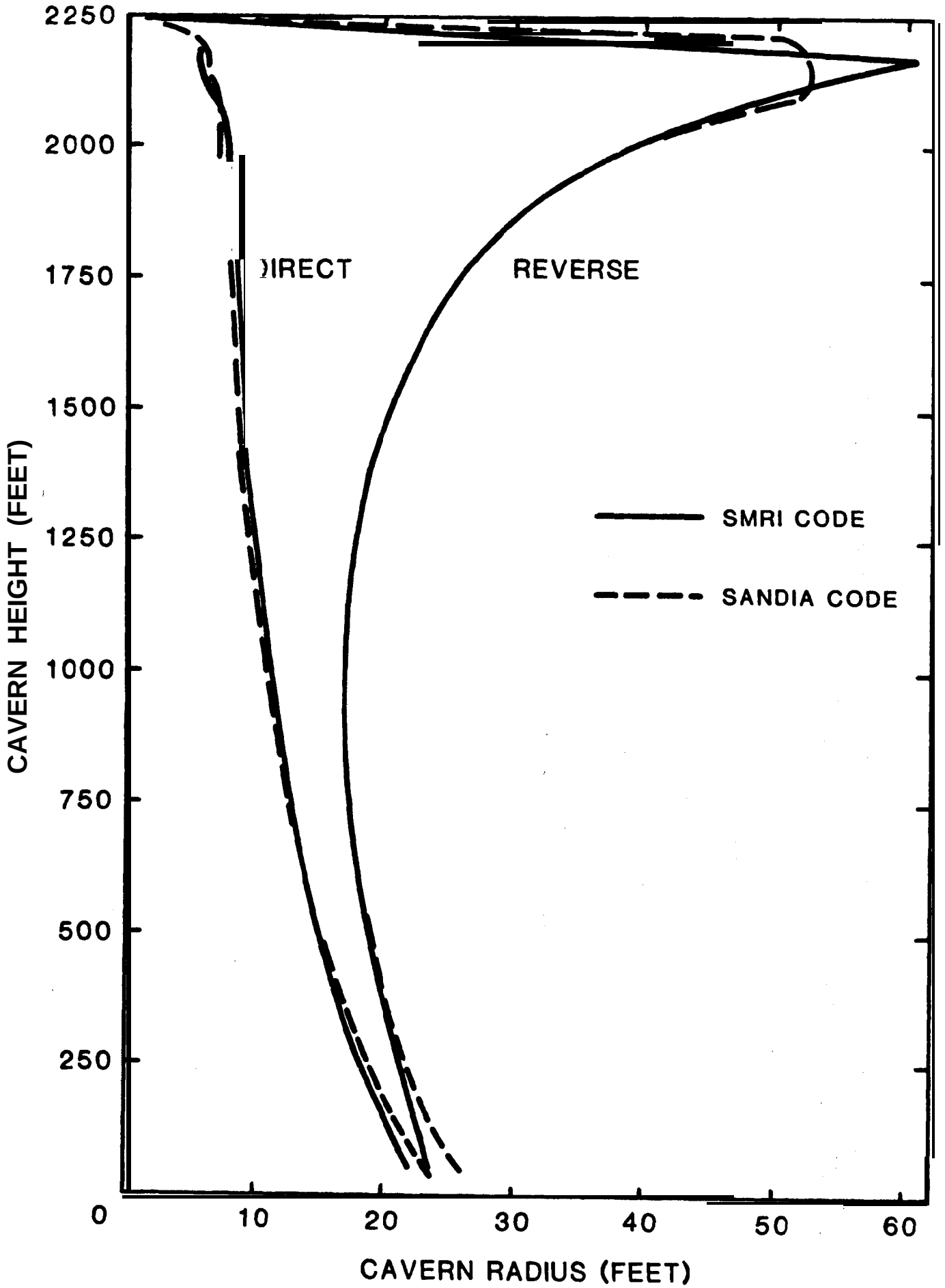

Figure 2. A Comparison of Calculated Cavern Shapes at 1322 gal/min

tubing was set at a depth of 4450 feet and a 10-3/4 inch production casing was set at a depth of 2280 feet. The initial borehole size was taken to be 15 inches in diameter. In actuality, the two wells would eventually coalesce with each other and with a third well started later therby forming Cavern 106. All simulations and data discussed here are for the period when each well forms a separate cavity. This case was simulated with both the SMRI code and the new code neglecting insolubles. The results are shown in Figure 3 along with sonar caliper data taken by the Dowel1 Corporation between July 2 and July 6, 1980. The radii data plotted in Figure 3 are effective radii, which, if the cavern cross section were circular give the same area as that measured (the same as the RMS radius). The calculated curves practically fall on each other, differing by 2% or less over the whole depth but both underestimate the measured volume by about 20%. This discrepancy could be caused by a number of factors. The assumed temperature for all calculations was 75°F but the exit temperature of the brine was as high as 98°F during some of the leaching. The insoluble.8 content was neglected (about 7%). The calculations assume an axisymmetric geometry but the actual cross sections were not circular. This fact can be significant because the larger surface to volume ratios would cause more salt to dissolve than was estimated. The sonar data was taken in eight directions, and if the average value of the radii are taken rather than the RMS value the results are quite different indicating a large deviation from circularity. Figure 4 shows the average radius data plotted with the calculated values. This plot indicates a'

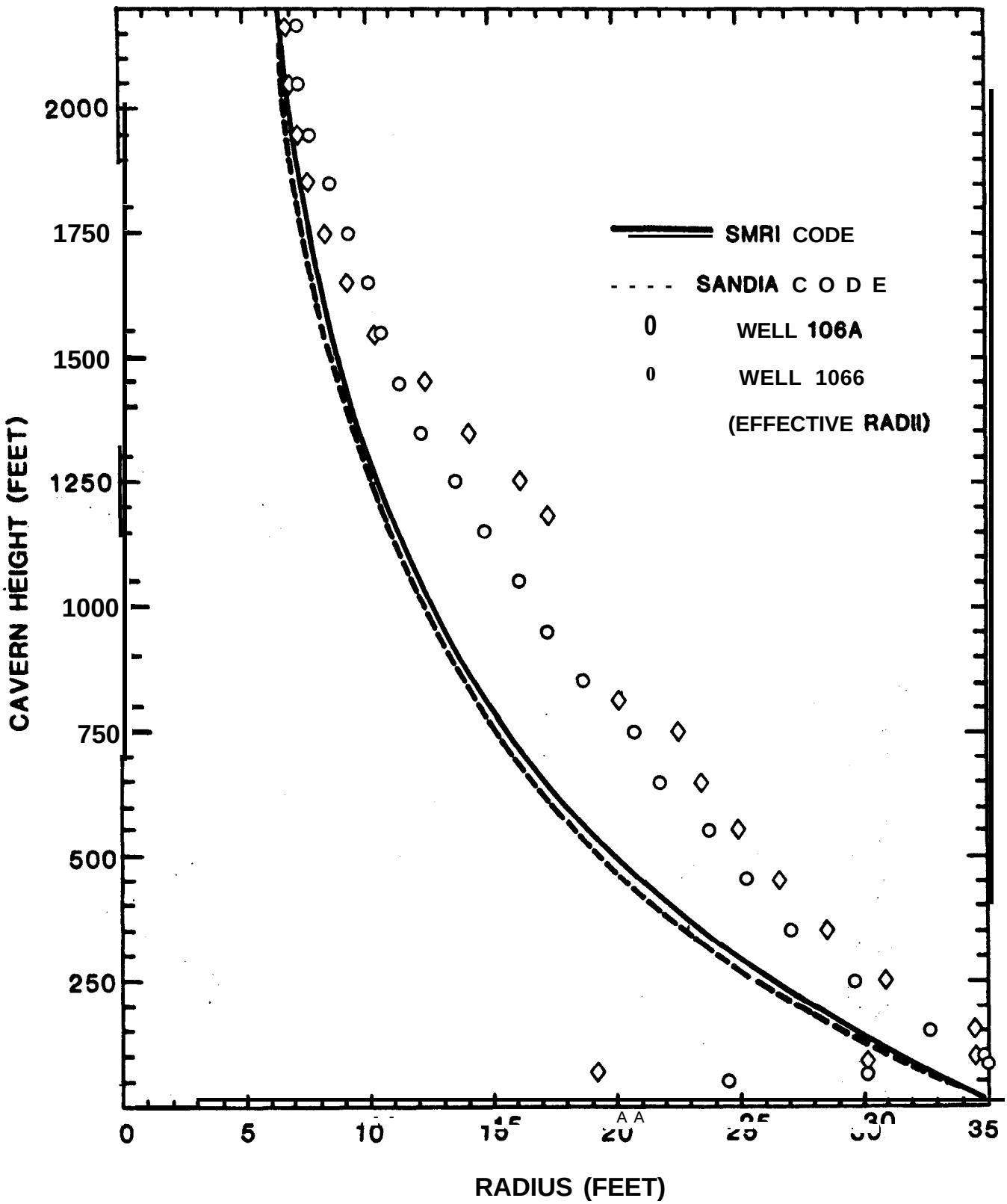

Figure 3. A Comparison of Calculated and Measured Cavern Shapes for Bryan Mound Cavern 106

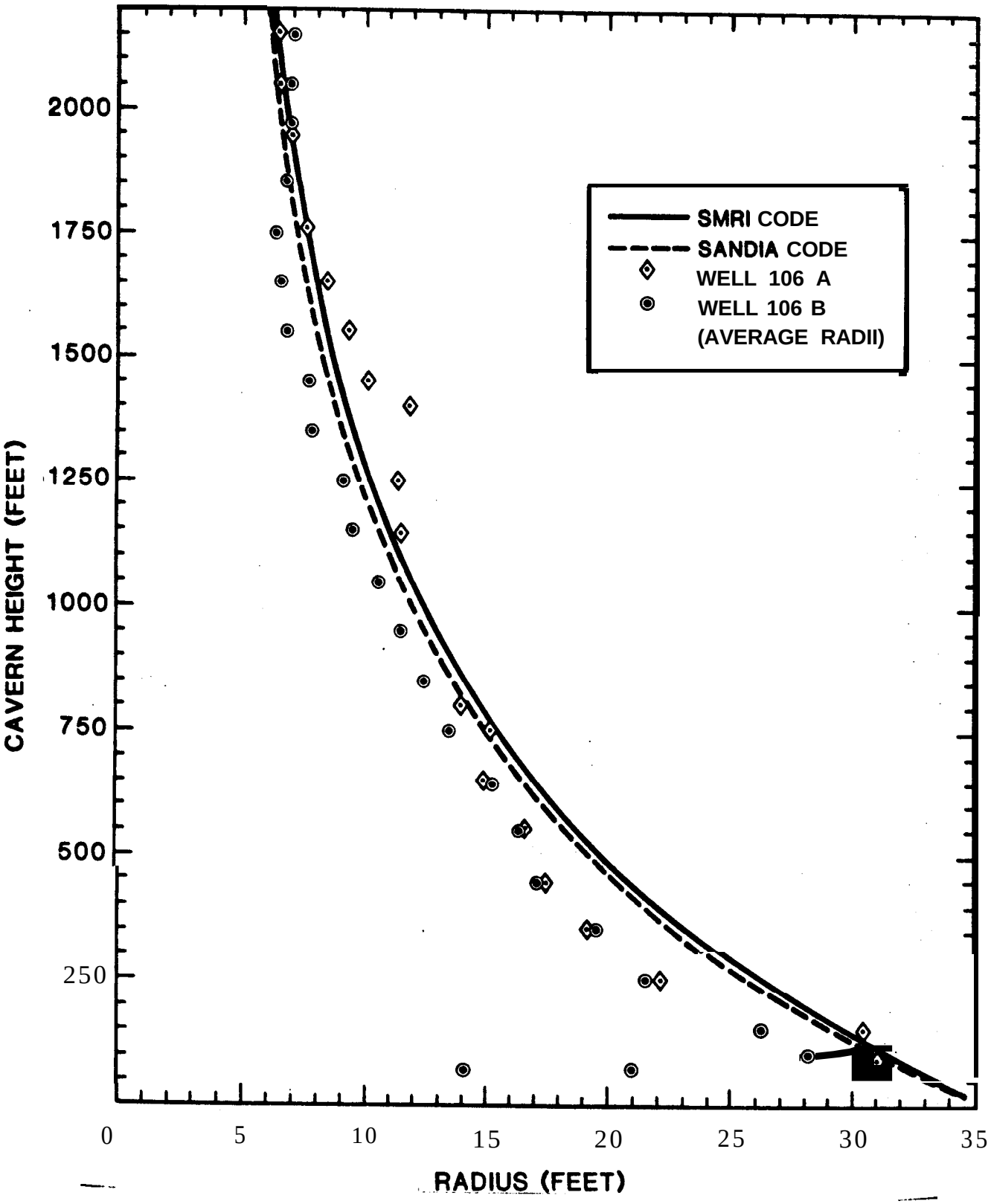

Figure 4. A Comparison of Calculated and Measured Shapes For Bryan Mound Cavern 106

better fit and the calculations even seem to overestimate the cavern size slightly. The asymmetries in the dissolution of the cavern can be caused by the presence of highly soluble sylvite deposits, uneven distribution of anhydrite or other insolubles, or uneven convective mixing of the injected water, none of which can be accounted for in an axisymmetric calculation. Considering all the assumptions that were made, the calculated results seem quite good.

Bryan Mound Cavern 104

Some data exists for a slightly different leaching configuration in Bryan Mound Well 104 B. At that cavern direct leaching was also employed but the production casing was placed well below the oil blanket and only 200 feet above the injection point which was at 4400 feet depth. The following raw water flow rates were estimated by Bryan Mound operations personnel for the 46 days prior to the first sonar caliper survey.

Day	Flow Rate (ft^3/hr)
1	970.5
2	10250.6
3	6192.1
4	10723.8
5 - 7	8437.9
8 - 11	7282.9
12 - 21	8678.5
22 - 23	8470.0
24 - 26	0.0
27 - 34	8470.0
35	9496.6
36 - 46	7282.9

Data from the Dowell Corporation sonar caliper survey of September 5, 1980 are shown in Figure 5 along with simulation results from the SMRI code and the Sandia Code. The radii plotted

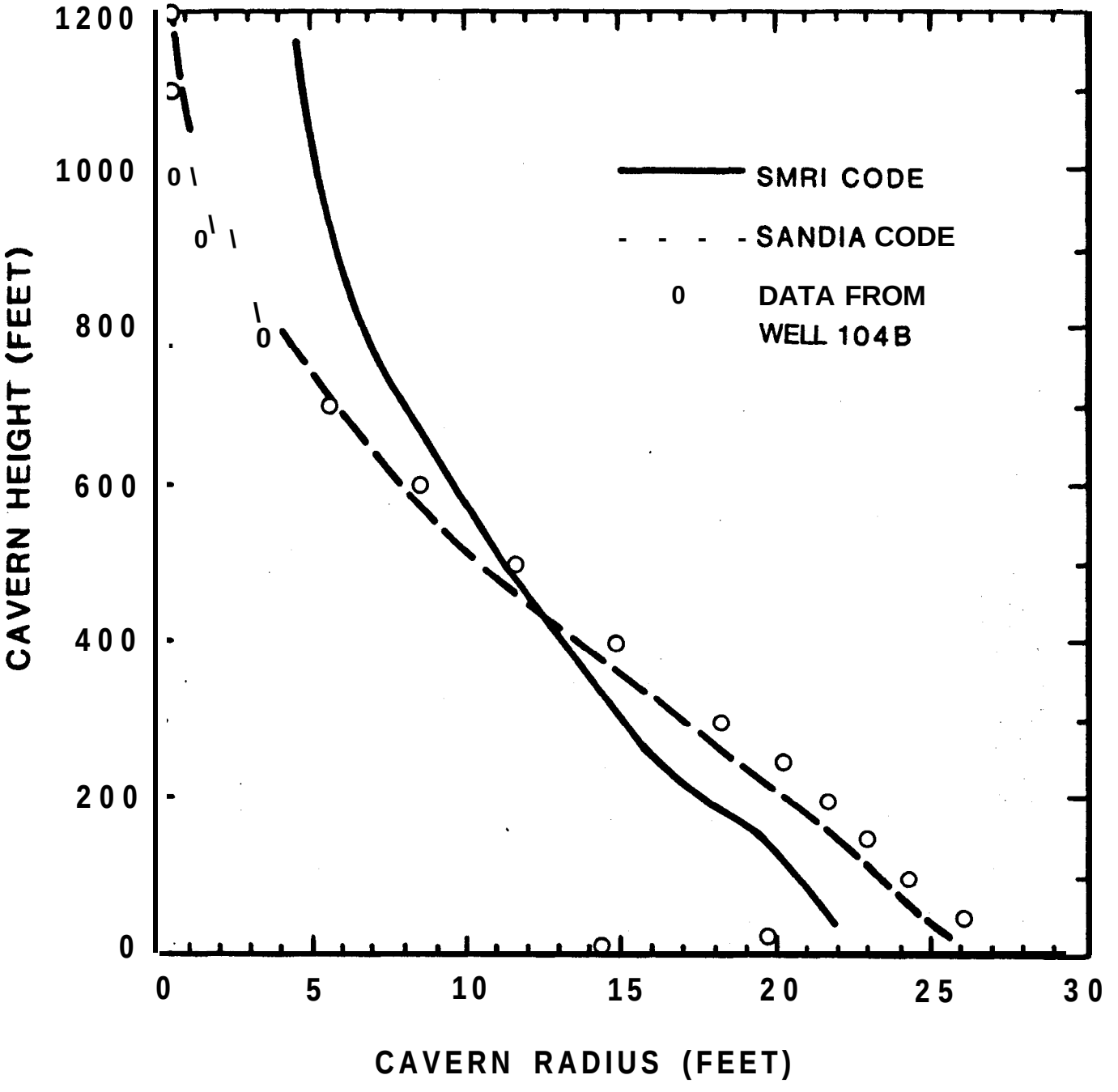

Figure 5. A Comparison of Calculated and Measured Cavern Shapes for Bryan Mound Well 104 B on September 5, 1980

are effective (RMS) values. Since the cross sections are nearly circular for this case, the average values are only slightly different. It is seen that the SMRI code significantly overpredicts the roof radius while underpredicting the cavern volume and base radius. The dissolution above the brine production level is determined by the mixing model. For the Sandia code mixing is based on the eddy diffusion model previously described. It appear8 that this model provides a close approximation to the actual mixing occurring in this leaching configuration. The same data is plotted in Figure 6, but the calculation8 shown include the effect of 7% insolubles. The version of the SMRI code that is available to us was not designed to include insoluble buildup so the calculations shown in Figure 6 were done using a modification incorporated by W. E. Wowak of Sandia National Laboratories. The inclusion of insolubles produce8 an even better fit to the data and improves confidence in the models used.

Leach-Fill Simulation

Unfortunately, no data are available at present to test the options for which the code was developed, namely the leach-fill and oil withdrawal modes. An example of each type of calculation will be given however to illustrate code capability and for comparison with future data.

The first example is for a leach-fill process in a full sized SPR cavern (nominal oil capacity = 10 million barrels). The cavern is assumed to have been solution mined to a volume of 4,383,800 barrels at the start time of the leach-fill process. The raw water injection is assumed constant at 32775 ft^3/hr

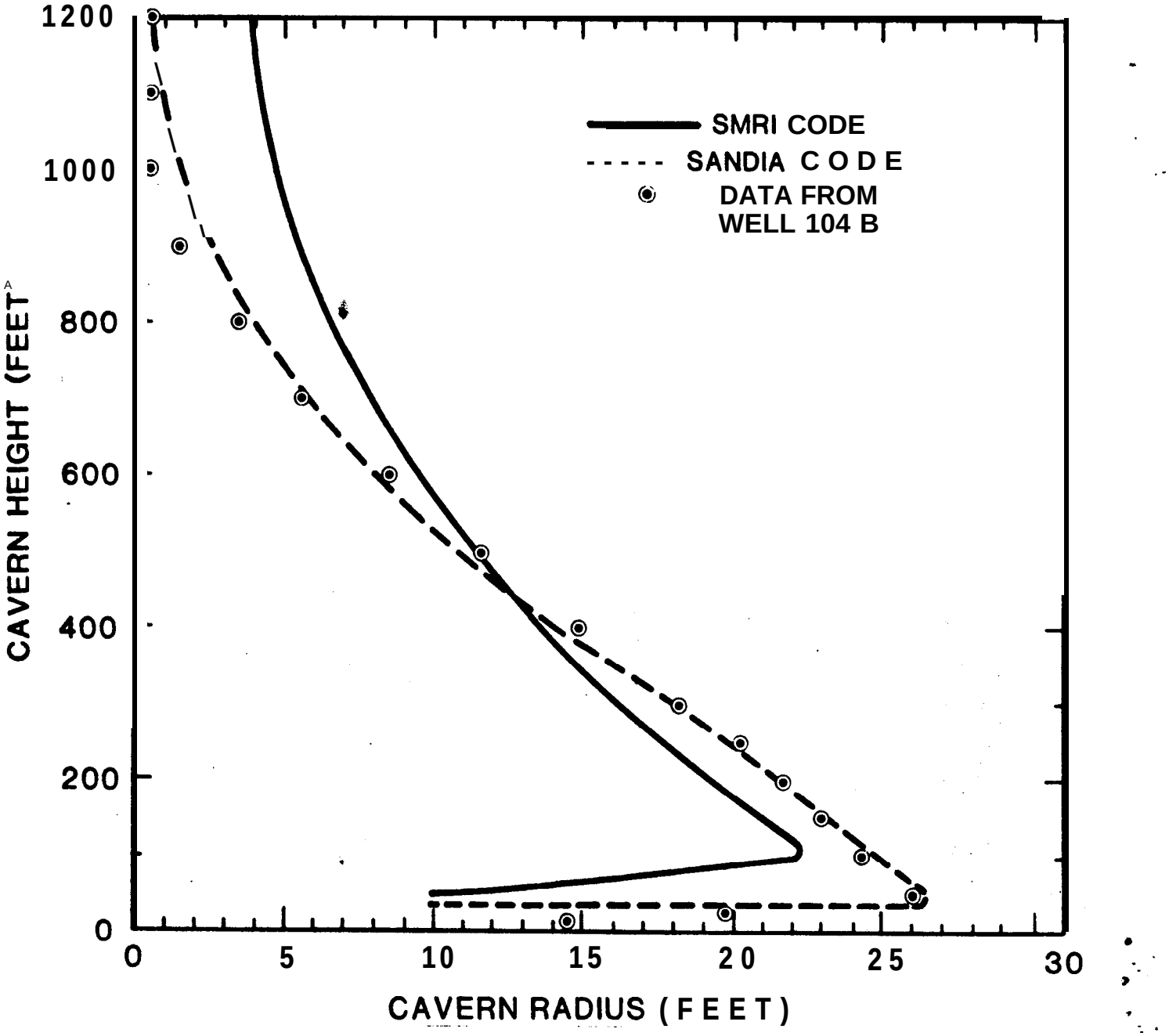

Figure 6. A Comparison of Calculated and Measured Cavern Shapes for Bryan Mound Well 104 B on September 5, 1980

(140,000 BPD), insolubles are neglected, and the following solution mining schedule is followed.

Flow Duration (Hours)	Injection Depth (feet)	Production Depth (Feet)	Oil Flow (Ft^3/Hr)
1680	2300	4100	0
3600	3100	4100	2644
1200	3100	4100	2995
2400	3800	4000	3744
7206	3800	4000	7206

The calculated cavern shape at the end of each of the above steps is shown in Figure 7. An approximation to the above process can be carried out with the SMRI code by sequencing a large number of runs. The method of adjusting the boundary conditions between runs will cause a slight underestimate of the cavern volume. Such a calculation for the above case has been carried out by H. C. Shefelbine of Sandia National Laboratories. The calculated cavern shape is similar to that in Figure 7, except that there is more volume near the top of the cavern and less near the bottom. The volume Shefelbine calculated is 12.2 million barrels, which is 4% lower than the 12.7 million barrels calculated with the Sandia code. Again there is good agreement with the expected result.

Oil Withdrawal Simulation

The final example is for five cycles of fill and withdrawal of oil in the standard SPR cavern of the previous example. It is assumed that.the 12.7 million barrel cavern contains 10 million barrels of oil and 2.7 million barrels of saturated brine. The oil-brine interface is 680 feet above the bottom of the cavern. Raw water (SG = 1.0108) injected at 49603 ft^3/hr at a height of

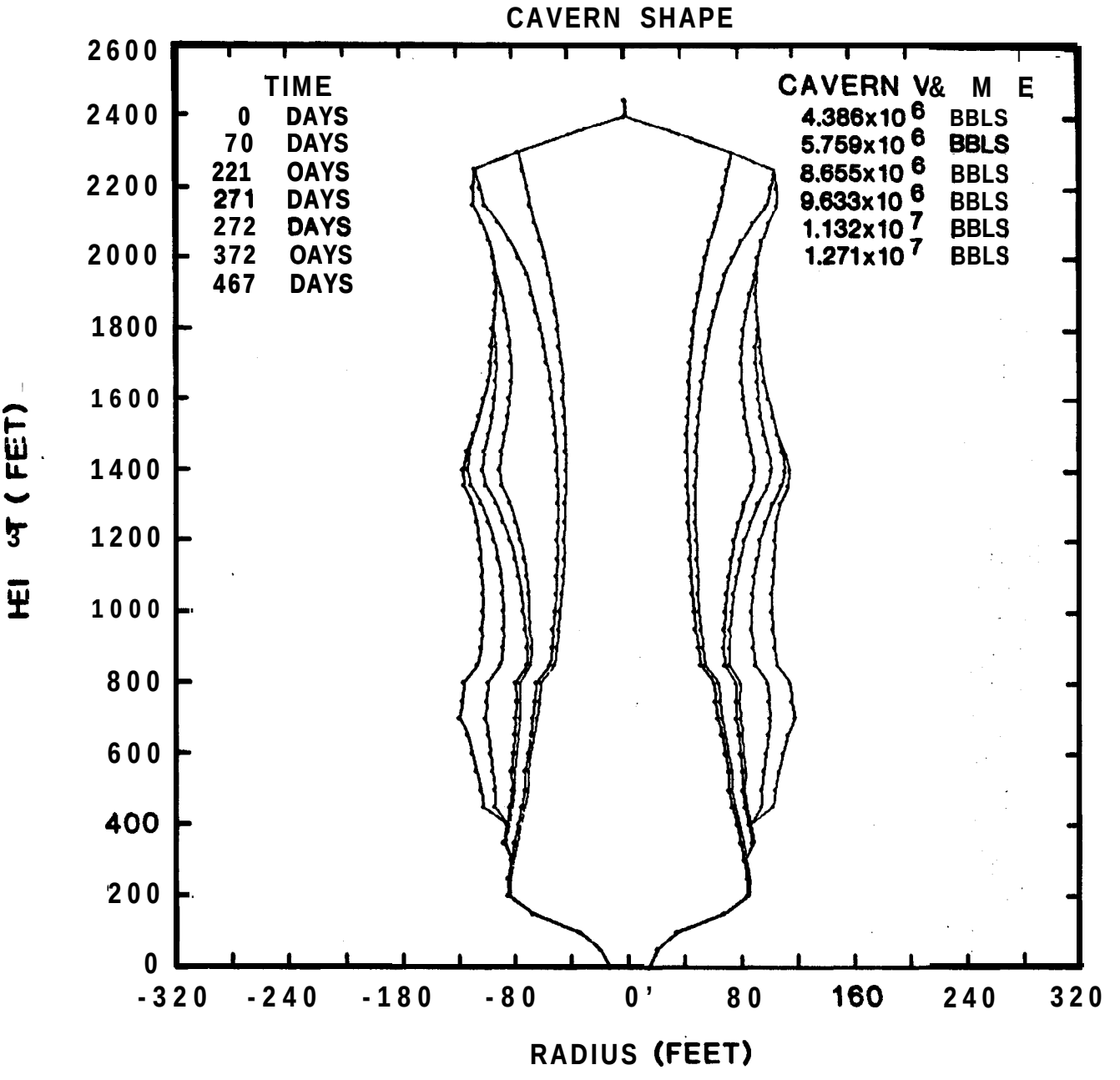

Figure 7. Calculated Cavern Shapes for the Leach-Fill Process Raw Water Injection Rate = 140,000 Barrels Per Day

400 feet is used to displace the oil until the interface moves to the top of the cavern (height = 2450 ft). A zero flow condition is then maintained for twenty days to allow the cavern brine to approach saturation (>90%). The cavern is then filled with oil again (instantly) and the withdrawal cycle, including the zero flow period is repeated. Figure 8 shows the initial cavern shape and the calculated shape after each withdrawal cycle. The cavern volumes for each curve are listed in Figure 8 from inner to outer curve. As expected, the region of the cavern just above the raw water injection level grows the fastest because it is exposed for a longer period of time to the lowest salinity brine.

It has been assumed in these calculations that when the oil is withdrawn the surface oil film covering the salt is quickly eroded and does not retard the dissolution of the freshly exposed salt surface. This assumption may not be valid (the exact mechanics of the film removal is not yet known) and if it is not valid the final shape can deviate significantly from that shown. When data on the film removal delay time becomes available the code can be modified to incorporate this effect.

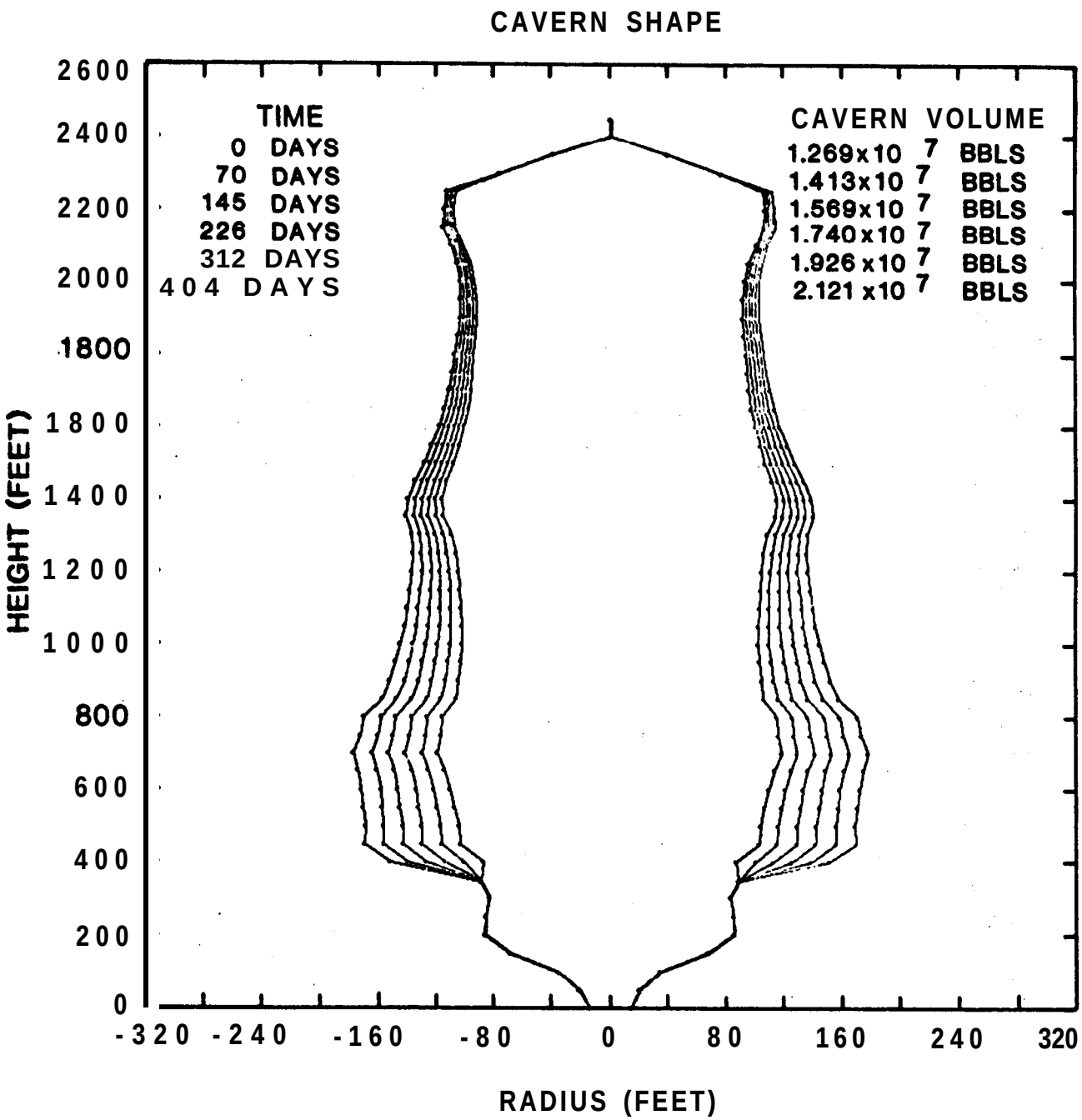

Figure 8. Calculated Cavern Profiles for Five Cycles of Oil Withdrawal From a Proposed SPR Cavern

CONCLUSIONS

A new solution mining code has been developed which is suitable for calculating cavern development in salt. The code is presently in usable form on the Sandia CDC 6600/7600 system. It is applicable to axisymmetric caverns having a single injection and production level. It has options of leaching with or without motion of the oil blanket so that leach-fill or oil withdrawal operations can be simulated. The raw water injection options include direct, reverse and zero flow conditions. If knowledge of the local insoluble8 content or salt dissolution rate is available, it can be incorporated into'the calculations.

Comparison of the code results with the SMRI solution mining code, SALT77, show very good agreement for four different examples considered. A fifth example, Bryan Mound Cavern 104 B, shows some deviation from the SMRI calculation but excellent agreement with the available data. Comparison of both codes with data from Bryan Mound wells 106 A and B show fair agreement despite the. fact that these wells deviate considerably from the axisymmetric assumption. Calculations which exercise the leach-fill and oil withdrawal options have been performed for a full sized SPR cavern but at present there is no way to evlauate their accuracy.

Several modifications or extensions to the code are being considered. These include, incorporation of well hydraulic calculations, automatic time step selection, a non-axisymmetric cavern option, and a better salt entrainment model.

REFERENCES

1. A Saberian and A. L. Podio, A Computer Model For Describing the Development of Solution-Mined Cavities, IN SITU, 1(1), p. 1-36 (1977).

2. B.R. Morton, et al., Turbulent Gravitational Convection From Maintained and Instantaneous Sources, Proc. of the Royal Society, Series A, Vol. 234, No. 1196, Jan 24, p. 1, (1956).

3. G. Walin, "Contained Non-Homogeneous Ffow Under Gravity or How to Stratify a Fluid in the Laboratory", v. Fluid Mech. 48, p. 647, (1971).

4. L. Rahm and G. Walin, 'Theory and Experiment on the Control of the Stratification in Almost Enclosed Containers," J. Fluid Mech. 90, p. 315 (1979).

5. L. Rahm and G. Walin, 'On Thermal Convection in Stratified Fluids", Geophys. Astrophys. Fluid Dynamics, V 13, p. 51 (1979).

6. R. N. Durie and F. W. Jessen, "Mechanism of the Dissolution of Salt in the Formation of Underground Salt Cavities', SPE Journal, p. 183, (June 1964).

7. R., W. Durie and F. W. Jessen, "The Influence of Surface Features in the Salt Dissolution Process", SPE Journal, p. 275 (September 1964).

8. J. S. Turner, Bouyancy Effects in Fluids, Cambridge Univ. Press, New York, 1973.

9. R. M. Knapp and A. L. Podio, "Investigation of Salt Transport in Vertical Boreholes and Brine Invasion Into Fresh Water Aquifers", ONWI-77 (May 1979).

10. M.S. Plesset and C. G. Whipple, 'Viscous Effects in Rayleigh-Taylor Instability", Phys. of Fluids Vol. 17, No. 1, p. 1 (January 1974).

11. B. J. Hill, 'Measurement of Local Entrainment Rate in the Initial Region of Axisymmetric Turbulent Air Jets', J. Fluid Mech. 51(4), p. 773, February 22, 1972.

DISTRIBUTION

US Department of Energy
Strategic Petroleum Reserve
Project Management Office
900 Commerce Road East
New Orleans, LA 70123
Attnr E. E. Chapple
C. C. Johnson
W. J. Smollen
G. A. Stafford
C. L. Steinkamp

US Department of Energy
Strategic Petroleum Reserve
1000 Independence Ave, SW
Washington, DC 20585
Attnt L. Pettis
R. Smith

Aerospace Corporation
880 Commerce Road West, Suite 300
New Orleans, LA 70123
Attnt K. Henrie
B. Merkle

Aerospace Corporation
P0 Box 92957
Loe Angeles, CA 90009
Attn: G. F. Kuncir

Dravo Utility Constructors, Inc.
850 S. Clearview Pkwy
New Orleans, LA 70123
Attnr R. Heaney (2)

Jacobs/D'Appolonia Engineers
6226 Jefferson Hwy, Suite B
New Orleans, LA 70123
Attnt H. Kubicek
P. Campbell

Gene Ford
P 0 Box 19672
Houston, TX 77024

Solution Mining Operations
and Sub Surface Storage
4148 Loire Dr
Kenner, LA 70062

A. Saberian & Associates
1701 Evergreen Avenue
Austin, TX 78704
Attnt A. Saberian
A. Podio

C. F. Chen
Department of Aerospace &
Mechanical Engineering
University of Arizona
Tucson, AZ 85721

Dr. P. Gnirk
RE/SPEC Inc.
P. 0. Box 725
Rapid City, SD 57701

4000 A. Narath
4500 E. H. Beckner
4540 M. L. Kramm
4543 J. F. Ney
4543 G. W. Whiting
5500 0. E. Jones
5510 D. B. Hayes
5512 D. F. McVey
5512 A. J. Russo (25)
5520 T. B. Lane
5530 W. Herrmann
5540 0. E. Jones (Acting)
8214 M. A. Pound
3141 L. J. Erickson (5)
3151 W. L. Garner (3)
(For DOE/TIC)
DOE/TIC (25)
(C. Dalin, 3154-4)